



# MANTA: A Large-Scale Multi-View and Visual-Text Anomaly Detection Dataset for Tiny Objects

## Supplementary Material

Lei Fan<sup>1</sup> \*

Dongdong Fan<sup>2</sup>

Zhiguang Hu<sup>3</sup>

Yiwen Ding<sup>2</sup>

Donglin Di<sup>4</sup>

Kai Yi<sup>5</sup>

Maurice Pagnucco<sup>1</sup>

Yang Song<sup>1</sup>

<sup>1</sup>UNSW Sydney <sup>2</sup>Gaozhe Technology <sup>3</sup>SACAU <sup>4</sup>Tsinghua University <sup>5</sup>University of Cambridge

<https://grainnet.github.io/MANTA>

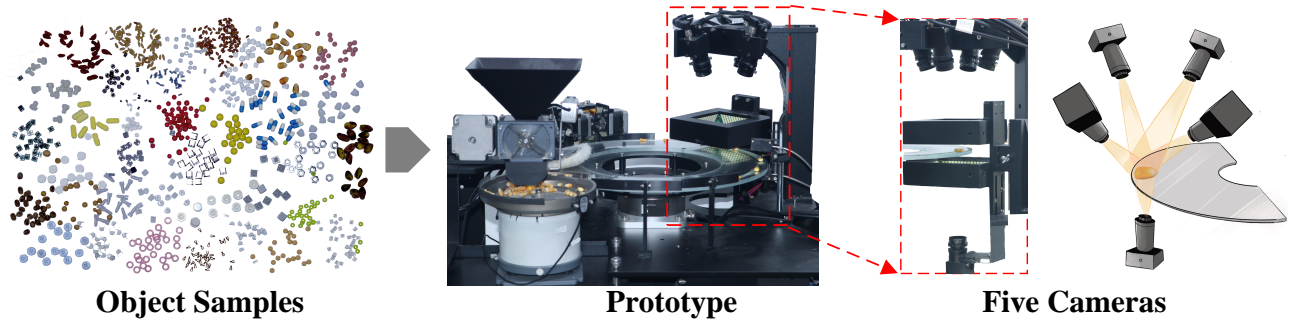


**Figure I. Multi-view images captured using the prototype.** The raw object samples were preprocessed to filter out apparent impurities before being individually fed into the device. The prototype is equipped with five high-resolution cameras. Four cameras are arranged in a quadrilateral formation, tilted downward at 30°, while one additional camera is positioned vertically beneath, pointing upward.

In this supplementary material, we provide a detailed description of MANTA and our benchmark. This document includes:

- Detailed information regarding data collection, sample visualizations, and statistical analysis of both visual and text components in **MANTA**, as provided in Section 1.
- Comprehensive benchmarking results, as provided in Section 2.
- Implementation details of advanced models, as discussed in Section 3.

## 1. MANTA

**Data acquisition** We presented detailed collected object samples and the structure of the prototype, as shown in Figure I. The raw object samples were preprocessed to remove apparent impurities before being introduced to the prototype. Each object was transferred onto a transparent plate and individually captured by the five cameras, providing comprehensive visual information.

**Visual Component** We showed the detailed dataset distribution, as presented in Table I, covering the normal and anomalous data across each domain and category, along with the split between training and testing sets. We also estimated the maximum bounding cuboid sizes in physical volume for each object type in the 38 categories and the storage requirements for image data in each domain. For each of the 38 categories, we randomly selected two normal and two anomalous samples, as illustrated in Figure II.

**Text Component** We provided detailed data distributions for the *Declarative Knowledge (DeclK)*, including both category-specific and domain-specific anomalies, as shown in Table II. We further visualized several examples of complete explicit instructions, reasoning processes, and concepts, encompassing both category-specific and domain-specific examples, as shown in Figure III.

For the *Constructivist Learning (ConsL)*, we provided detailed data distributions, including combinations of varying difficulty levels with different Normal-Normal (N-N) and Normal-Anomaly (N-A) image pairs for each category, as shown in Table III. Additionally, we showcased multiple-choice questions (MCQs) of varying difficulty levels across

\*Corresponding author: lei.fan1@unsw.edu.au

different domains, along with their corresponding conclusions, as illustrated in Figure IV.

## 2. Detailed Results

We provided specific experimental results across multiple benchmarking experiments:

- Table IV provides detailed results corresponding to **Table 2**, using the *single-view* setting for each class. Each view of multi-view images is treated as an independent training sample. Detailed results are reported in terms of I-/P-AUROC for each category.
- Table V presents detailed results corresponding to **Table 3**, using the *multi-view* setting for each class. Multi-view images are directly used to train the models. Due to memory limitations, several advanced models were modified to adapt to the multi-view setting. Results are reported in terms of I-/P-AUROC for each category.
- Table VI shows detailed results corresponding to **Table 4**, using the *multi-class* setting. Multiple categories within the same domain are mixed, and each view is treated as a training sample. Detailed results are reported in terms of I-/P-AUROC for each category.
- Table VII provides detailed results corresponding to **Figure 9**, using *text-prompt* setting. Text information provided in the Declarative Knowledge is used to train the anomaly detection model. Results are reported in terms of I-/P-AUROC for each category.

## 3. Implementation Details

### 3.1. Single-class Models

We provided detailed experimental settings for various benchmarking models under *single-view* and *multi-view* settings. Typically, we leveraged the official code for each method to evaluate the models. The inputs were resized as  $224 \times 224$  for *single-view* and  $224 \times 1120$  for *multi-view*.

- RD [2]: The model was trained for 40 epochs with a batch size of 8. The Adam optimizer [7] was employed, the learning rate was set to 0.005, the Cosine Similarity loss function was utilized, and Wideresnet50 [5] was selected as the backbone.
- PatchCore [16]: The model operated with a batch size of 16. The backbone is Wideresnet50 [5], utilizing layers 2 and 3. Notably, the percentage parameter was set to 0.01 for sample selection. To prevent memory overflow, coresnet operations are executed after processing every  $batch\_size \times batch\_size$  samples.
- CDO [1]: The model was trained for 100 epochs with a batch size of 16. The AdamW optimizer [13] was employed with a weight decay of 0.0001. The learning rate was initialized at  $4 \times 10^{-4}$ , using ExponentialLR with  $\gamma = 0.95$ . HRNet32 [19] was utilized as the backbone.

- DMAD [11]: We used the PPDM version. The model was trained for 50 epochs with a batch size of 4. The AdamW optimizer [13] was used, and the learning rate was initialized at 0.005, using CosineAnnealingLR with  $T_{max} = 50$ . The Cosine Similarity loss function was employed, and Wideresnet50 [5] was utilized as the backbone.
- SimpleNet [12]: It consists of a two-stage training process, with 20 meta-training epochs and 4 GAN-training epochs. A batch size of 16 is used. The backbone is a Wideresnet50 [5], with its feature extraction layers frozen during training. A discriminator with 2 layers and a hidden dimension of 1024 is optimized using Adam (weight decay  $1 \times 10^{-5}$ ) [7] with a learning rate of 0.0002. The discriminator incorporates a margin threshold ( $dsc\_margin = 0.15$ ) and Gaussian noise ( $noise\_std = 0.05$ ) for robustness. Additionally, a pre-projector with a dimension of 1536 is optimized using Adam with a learning rate of  $1 \times 10^{-4}$ .

### 3.2. Multi-class Models

We provided detailed experimental settings for various benchmarking models under *multi-class* setting. Typically, we leveraged the official code for each method to evaluate the models. The inputs were resized as  $224 \times 224$  for the *single-view* training.

- UniAD [21]: The model was trained for 50 epochs with a batch size of 32. The optimizer used was AdamW [13] with a learning rate of  $4 \times 10^{-4}$ ,  $\beta$ -parameters [0.9, 0.999], and a weight decay of 0.0001. The learning rate was scheduled using StepLR with a step size of 800 and a decay factor  $\gamma = 0.1$ . The loss function employed was FeatureMSELoss. The backbone was EfficientNet-B4 [18], utilizing layers 1, 2, 3, and 4.
- CRAD [8]: The model was trained for 20 epochs with a batch size of 8. The optimizer used was AdamW [13], with separate learning rates for different parameters:  $grid\_lr = 0.1$  for trainable query parameters and  $net\_lr = 0.001$  for other parameters. The learning rate scheduler was StepLR, with a step size of 40 and a decay factor  $\gamma = 0.1$ . The loss function employed was FeatureMSELoss. The backbone was EfficientNet-B4 [18], using layers 3 and 4.
- HGAD [20]: The backbone used is EfficientNet-b6 [18], and the flow model is a conditional-flow model [4] with 12 coupling layers and a clamping hyperparameter ( $clamp\_alpha = 1.9$ ). Features are extracted from 3 levels. Training consists of two stages: 10 meta-epochs and 8 sub-epochs. The batch size is set to 8. The optimizer is Adam [7] with a learning rate of  $2 \times 10^{-4}$ . Learning rate decay is applied at epochs 50, 75, and 90 with a decay rate of 0.1. Additionally, a warming-up phase is employed with a warm-up period of 2 epochs.

### 3.3. Text-prompt Models

We provided detailed experimental settings for various benchmarking models under *text-prompt* setting. Typically, we leveraged the official code for PromptAD and VCP-CLIP to evaluate the models.

- WinCLIP [6]: We used an unofficial code<sup>1</sup>. The batch size was set to 1, and a  $k$ -shot setting with  $k = 1$  was used to construct the normal reference image feature memory. The input image size was  $240 \times 240$ , with ViT-B-16-plus-240 [3] as the image encoder and laion400m-e31 [17] as the text encoder. For textual input, universal nouns and adjectives were combined with domain-specific nouns and adjectives to create descriptive phrases. Anomalous phrases were formatted as “category with noun” and “adjective category”, while normal phrases follow the format “category without noun”. All phrases are directly tokenized without any sampling or filtering.
- PromptAD [10]: The model was trained for 20 epochs with a batch size of 256 and a  $k$ -shot setting of  $k = 1$ . The input image size was set to  $240 \times 240$ , with ViT-B-16-plus-240 [3] as the image encoder and laion400m-e31 [17] as the text encoder. The optimizer used is SGD, configured with a learning rate of 0.002, momentum of 0.9, and a weight decay of 0.0005. The learning rate scheduler was CosineAnnealingLR, with  $T_{\max} = 20$  and  $\eta_{\min} = 1 \times 10^{-5}$ .
- VCP-CLIP [14]: The model was trained for 2 epochs with a batch size of 32 and a  $k$ -shot setting of  $k = 1$ . The input image size is  $518 \times 518$ , with ViT-L-14-336 [3] as the image encoder and CLIP text encoder [15]. The learning rate is set to 0.00004. The text setup includes a single token and a learnable text prompt embedding with 11 layers. To prevent memory overflow, 10 normal texts and 10 anomalous texts are randomly sampled and tokenized for each run.

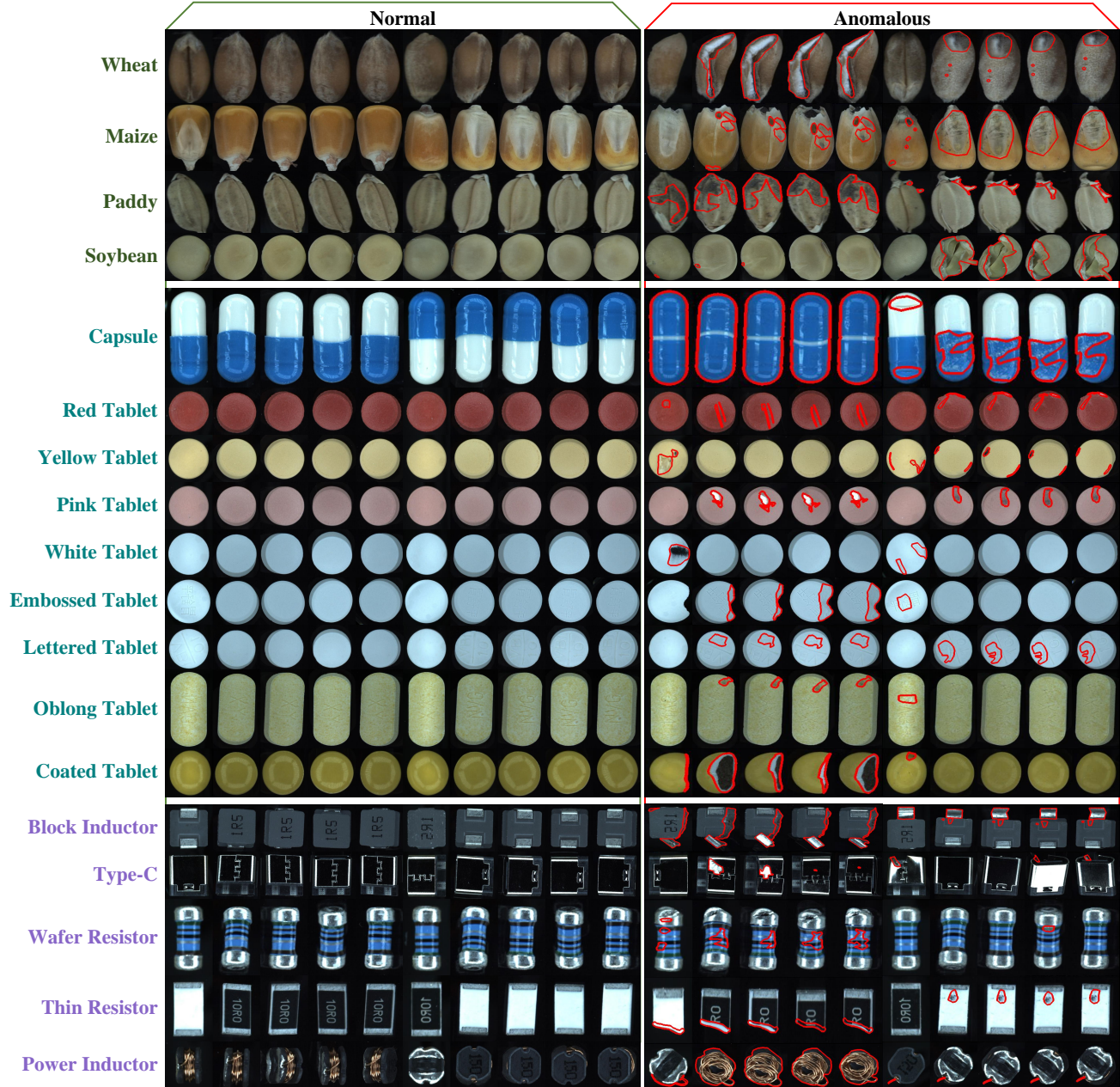
### 3.4. Visual-Language Model

Our baseline employed BLIP-2 [9] as the backbone. In the zero-shot setting, a specific test sample was selected, and the input data was constructed by concatenating the reference image and the test image into a single composite image. The model was then prompted to generate predictions. In the few-shot setting, one question-and-answer pair is randomly chosen and assigned to the test image. The model is trained for 11 epochs. During testing, the reference image and test image are concatenated into a composite image, and the model is prompted to generate predictions.

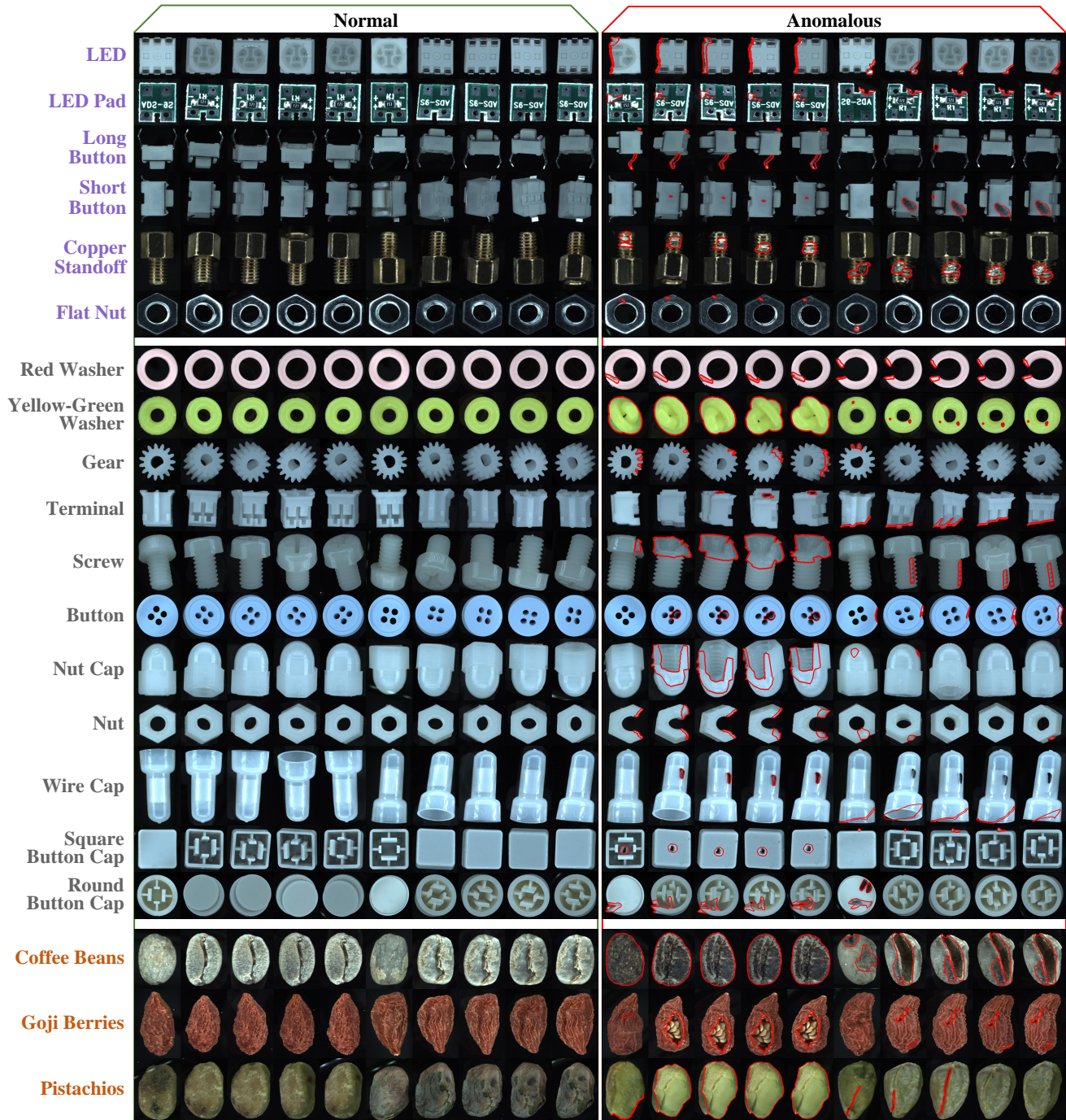
---

<sup>1</sup><https://github.com/mala-lab/WinCLIP>





(a) Normal and anomalous samples for 4, 9, 5 categories in the Agriculture, Medicine, and Electronics domain respectively.



(b) Normal and anomalous samples for 6, 11, 3 categories in the Electronics, Mechanics, and Groceries domain respectively.

**Figure II. Normal and anomalous samples for each of the 38 categories across five domains.** It includes two subfigures (a) and (b). Annotated anomalous regions are highlighted with red contours, and the original images are resized to enhance visualization clarity.

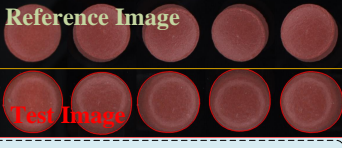
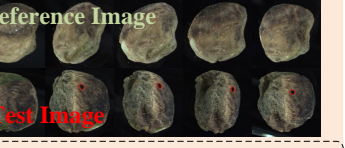
Table II. **Detailed data distribution of the *Declarative Knowledge* in MANTA.** It comprises 391 category-specific and 484 domain-specific anomalies, covering 38 categories across five domains.

Domain	Category	Category-specific Anomalies	Domain-specific Anomalies	Domain Total
Agriculture	Wheat	13	130	191
	Maize	14		
	Paddy	22		
	Soybean	12		
Medicine	Capsule	28	106	170
	Red Tablet	2		
	Yellow Tablet	2		
	Pink Tablet	2		
	White Tablet	2		
	Embossed Tablet	7		
	Lettered Tablet	10		
	Oblong Tablet	7		
	Coated Tablet	4		
Electronics	Block Inductor	7	70	182
	Type-C	4		
	Wafer Resistor	10		
	Thin Resistor	10		
	Power Inductor	14		
	LED	6		
	LED Pad	25		
	Long Button	12		
	Short Button	11		
	Copper Standoff	7		
	Flat Nut	6		
Mechanics	Red Washer	15	90	216
	Yellow-Green Washer	15		
	Gear	17		
	Terminal	6		
	Screw	6		
	Button	23		
	Nut Cap	8		
	Nut	4		
	Wire Cap	10		
	Square Button Cap	11		
	Round Button Cap	11		
	Total	391		
Groceries	Coffee Beans	12	88	116
	Goji Berries	8		
	Pistachios	8		

<p>"domain": "agriculture", "domain-specific": "pest-ridden",</p> <p>"Reasoning": "caused by insect infestations that damage the kernel, leading to discoloration and decay".</p> <p>"Concepts": "color": "discolored, often yellow or brown", "location": "scattered across the kernel surface", "area size": "variable, from small spots to larger areas", "shape": "irregular patches or lesions", "quantity": "multiple, can cover significant areas",</p>	<p>"domain": "agriculture", "domain-specific": "sprouting",</p> <p>"Reasoning": "it indicates that the seed has absorbed moisture and is beginning to germinate, which is a natural developmental process under suitable conditions".</p> <p>"Concepts": "color": "green or pale green", "location": "emerging from seed coat", "area size": "small, linked to seed size", "shape": "cylindrical or elongated", "quantity": "one to several sprouts",</p>	<p>"domain": "medicine", "domain-specific": "crack",</p> <p>"Reasoning": "stress or impact causing a crack to form in the tablet".</p> <p>"Concepts": "color": "darker pink or grayish around crack", "location": "surface area", "area size": "varies with crack length", "shape": "linear or jagged line", "quantity": "single or multiple cracks",</p>
<p>"domain": "electronics", "domain-specific": "fragmented",</p> <p>"Reasoning": "mechanical stress or impact causing physical breakage".</p> <p>"Concepts": "color": "same as standard button color", "location": "surface area or body", "area size": "small to medium", "shape": "irregular fragments", "quantity": "one or more fragments",</p>	<p>"domain": "mechanics", "domain-specific": "abrasion",</p> <p>"Reasoning": "friction from repeated use or contact with rough surfaces, leading to surface wear".</p> <p>"Concepts": "color": "original color or faded areas", "location": "surface of the button cap", "area size": "variable, small to medium abrasion spots", "shape": "flat or slightly indented areas", "quantity": "single or multiple abrasions",</p>	<p>"domain": "groceries", "domain-specific": "deformation",</p> <p>"Reasoning": "genetic variation, environmental stress, or physical pressure during growth".</p> <p>"Concepts": "color": "green or pale", "location": "nut inside the shell", "area size": "variable, can affect part or all of the nut", "shape": "misshapen or warped", "quantity": "single or multiple nuts affected",</p>
<p>"domain": "agriculture", "category": "maize", "category-specific": "mildew",</p> <p>"Reasoning": "it is caused by fungal pathogens, primarily from the genus <i>Erysiphe</i>, which thrive in humid conditions and lead to a powdery fungal growth on the seed surface".</p> <p>"Concepts": "color": "white to gray powdery coating", "location": "surface of the kernel", "area size": "variable, can cover small to large areas", "shape": "powdery or fuzzy appearance", "quantity": "variable, may cover several kernels",</p>	<p>"domain": "medicine", "category": "capsule", "category-specific": "cap-body splitting",</p> <p>"Reasoning": "improper sealing or stress during processing leading to separation of the capsule cap from the body".</p> <p>"Concepts": "color": "same as capsule body color", "location": "joining area of cap and body", "area size": "varies with split length", "shape": "uneven or jagged split", "quantity": "single or multiple splits",</p>	<p>"domain": "medicine", "category": "white tablet", "category-specific": "humidity",</p> <p>"Reasoning": "exposure to excessive moisture causing degradation or alteration in tablet surface appearance".</p> <p>"Concepts": "color": "dull or slightly yellowish", "location": "surface area", "area size": "small spots or patches", "shape": "surface irregularities or blisters", "quantity": "few to several affected areas",</p>
<p>"domain": "electronics", "category": "copper standoff", "category-specific": "damaged threads",</p> <p>"Reasoning": "impact or pressure applied during handling or assembly".</p> <p>"Concepts": "color": "same as standard color of copper standoff", "location": "threaded area", "area size": "small", "shape": "abraded or deformed threads", "quantity": "one or more threads damaged",</p>	<p>"domain": "mechanics", "category": "gear", "category-specific": "tooth loss",</p> <p>"Reasoning": "excessive wear, mechanical stress, or improper alignment leading to tooth detachment".</p> <p>"Concepts": "color": "gray or metallic", "location": "edge of gear teeth", "area size": "scattered or dense tooth areas", "shape": "jagged or uneven edge", "quantity": "single or multiple teeth",</p>	<p>"domain": "groceries", "category": "coffee beans", "category-specific": "spoilage",</p> <p>"Reasoning": "decomposition due to improper storage conditions, such as excessive moisture or heat".</p> <p>"Concepts": "color": "dark brown or black", "location": "surface of the beans", "area size": "variable, often patchy", "shape": "soft or mushy spots", "quantity": "single or multiple beans affected",</p>

**Figure III. Examples in Declarative Knowledge.** Both domain-specific and category-specific anomalies are shown in complete explicit instructions, reasoning, and concepts. Each concept includes five visual attributes: color, location, area size, shape, and quantity.



<p>"domain": "agriculture",      "category": "wheat",      "difficulty": "N-N",</p> 	<p>"domain": "agriculture",      "category": "paddy",      "difficulty": "N-N",</p> 
<p>"Q1": "Is the image normal?",      "answer": true,      "Q2": "Is there a disease spot?",      "answer": false,      "Q3": "Are there any pest damages?",      "answer": false,      "Q4": "Is there any mold?",      "answer": false,      "Q5": "Is it free of shriveling?",      "answer": true,      "conclusion": "The wheat grains shown in the image are normal, with no anomalies such as disease spots, pest damages, mold, or shriveling."</p>	<p>"Q1": "Are there any spot anomalies in this image?",      "answer": false,      "Q2": "Is there any sign of mold in this image?",      "answer": false,      "Q3": "Is this image normal?",      "answer": true,      "Q4": "Is it free of pest damage in this image?",      "answer": true,      "Q5": "Are there any crack anomalies in this image?",      "answer": false,      "conclusion": "This rice image is normal, with no abnormalities observed, and no signs of spots, pests, or cracks."</p>
<p>"domain": "medicine",      "category": "red tablet",      "difficulty": "N-A, easy",</p> 	<p>"domain": "electronics",      "category": "block inductor",      "difficulty": "N-A, easy",</p> 
<p>"Q1": "Are there any swelling anomalies in this image?",      "answer": true,      "Q2": "Is there a disease spot?",      "answer": false,      "Q3": "Are there no signs of shriveling?",      "answer": true,      "Q4": "Is there no heat damage in the image?",      "answer": true,      "Q5": "Are there signs of mold?",      "answer": false,      "conclusion": "The five views show swelling abnormalities mainly concentrated on the left and right sides of views 1, 3, 4, and 5. The shape is clearly different from normal grains, and there are no signs of disease spots, shriveling, heat damage, or mold."</p>	<p>"Q1": "Anything anomalous?",      "answer": true,      "Q2": "Is there any mutilation?",      "answer": true,      "Q3": "Are there any cracks?",      "answer": false,      "Q4": "Is it free of blemishes?",      "answer": false,      "Q5": "Are there any foreign objects?",      "answer": false,      "conclusion": "In this image, mutilations are visible in the 2nd, 3rd, 4th, and 5th views, located at the lower left and below, showing irregular gaps that indicate the integrity of this electronic component is compromised. No signs of cracks or foreign objects are present, thus these two anomalies do not exist."</p>
<p>"domain": "mechanics",      "category": "terminal",      "difficulty": "N-A, hard",</p> 	<p>"domain": "groceries",      "category": "pistachios",      "difficulty": "N-A, hard",</p> 

**Figure IV. Examples in Constructivist Learning.** Each multiple-choice question comprises a pair of images, five questions, and a conclusion. The reference image, which is normal, serves as the image prompt, while the questions are designed to be answered based on the test image. For easy-level questions, a total conclusion is provided. For hard-level questions, a detailed conclusion is provided for each question. N-A denotes Normal-Anomaly image pairs.









## References

- [1] Yunkang Cao, Xiaohao Xu, Zhaoge Liu, and Weiming Shen. Collaborative discrepancy optimization for reliable image anomaly localization. *IEEE Transactions on Industrial Informatics*, 19(11):10674–10683, 2023. [2](#), [11](#), [12](#)
- [2] Hanqiu Deng and Xingyu Li. Anomaly detection via reverse distillation from one-class embedding. In *CVPR*, pages 9737–9746, 2022. [2](#), [11](#), [12](#)
- [3] Alexey Dosovitskiy. An image is worth 16x16 words: Transformers for image recognition at scale. *arXiv preprint arXiv:2010.11929*, 2020. [3](#)
- [4] Denis Gudovskiy, Shun Ishizaka, and Kazuki Kozuka. Cflow-ad: Real-time unsupervised anomaly detection with localization via conditional normalizing flows. In *WACV*, pages 98–107, 2022. [2](#)
- [5] Kaiming He, Xiangyu Zhang, Shaoqing Ren, and Jian Sun. Deep residual learning for image recognition. In *CVPR*, pages 770–778, 2016. [2](#)
- [6] Jongheon Jeong, Yang Zou, Taewan Kim, et al. Winclip: Zero-/few-shot anomaly classification and segmentation. In *CVPR*, pages 19606–19616, 2023. [3](#), [14](#)
- [7] Diederik P Kingma. Adam: A method for stochastic optimization. *arXiv preprint arXiv:1412.6980*, 2014. [2](#)
- [8] Joo Chan Lee, Taejune Kim, Eunbyung Park, Simon S. Woo, and Jong Hwan Ko. Continuous memory representation for anomaly detection. *ECCV*, 2024. [2](#), [13](#)
- [9] Junnan Li, Dongxu Li, Silvio Savarese, and Steven Hoi. Blip-2: Bootstrapping language-image pre-training with frozen image encoders and large language models. In *ICML*, pages 19730–19742. PMLR, 2023. [3](#)
- [10] Xiaofan Li, Zhizhong Zhang, Xin Tan, Chengwei Chen, Yanyun Qu, Yuan Xie, and Lizhuang Ma. Promptad: Learning prompts with only normal samples for few-shot anomaly detection. In *CVPR*, pages 16838–16848, 2024. [3](#), [14](#)
- [11] Wenrui Liu, Hong Chang, Bingpeng Ma, Shiguang Shan, and Xilin Chen. Diversity-measurable anomaly detection. In *CVPR*, pages 12147–12156, 2023. [2](#), [11](#), [12](#)
- [12] Zhikang Liu, Yiming Zhou, Yuansheng Xu, and Zilei Wang. Simplenet: A simple network for image anomaly detection and localization. In *CVPR*, pages 20402–20411, 2023. [2](#), [11](#)
- [13] I Loshchilov. Decoupled weight decay regularization. *arXiv preprint arXiv:1711.05101*, 2017. [2](#)
- [14] Zhen Qu, Xian Tao, Mukesh Prasad, Fei Shen, Zhengtao Zhang, Xinyi Gong, and Guiuguang Ding. Vcp-clip: A visual context prompting model for zero-shot anomaly segmentation. *ECCV*, 2024. [3](#), [14](#)
- [15] Alec Radford, Jong Wook Kim, Chris Hallacy, Aditya Ramesh, Gabriel Goh, Sandhini Agarwal, Girish Sastry, Amanda Askell, Pamela Mishkin, Jack Clark, et al. Learning transferable visual models from natural language supervision. In *ICML*, pages 8748–8763. PMLR, 2021. [3](#)
- [16] Karsten Roth, Latha Pemula, Joaquin Zepeda, Bernhard Schölkopf, Thomas Brox, and Peter Gehler. Towards total recall in industrial anomaly detection. In *CVPR*, pages 14318–14328, 2022. [2](#), [11](#), [12](#)
- [17] Christoph Schuhmann, Richard Vencu, Romain Beaumont, Robert Kaczmarczyk, Clayton Mullis, Aarush Katta, Theo Coombes, Jenia Jitsev, and Aran Komatsuzaki. Laion-400m: Open dataset of clip-filtered 400 million image-text pairs. *arXiv preprint arXiv:2111.02114*, 2021. [3](#)
- [18] Mingxing Tan and Quoc Le. Efficientnet: Rethinking model scaling for convolutional neural networks. In *ICML*, pages 6105–6114. PMLR, 2019. [2](#)
- [19] Jingdong Wang, Ke Sun, Tianheng Cheng, Borui Jiang, Chaorui Deng, Yang Zhao, Dong Liu, Yadong Mu, Mingkui Tan, Xinggang Wang, et al. Deep high-resolution representation learning for visual recognition. *PAMI*, 43(10):3349–3364, 2020. [2](#)
- [20] Xincheng Yao, Ruqi Li, Zefeng Qian, Lu Wang, and Chongyang Zhang. Hierarchical gaussian mixture normalizing flows modeling for unified anomaly detection. In *ECCV*, 2024. [2](#), [13](#)
- [21] Zhiyuan You, Lei Cui, Yujun Shen, Kai Yang, Xin Lu, Yu Zheng, and Xinyi Le. A unified model for multi-class anomaly detection. *NeurIPS*, 35:4571–4584, 2022. [2](#), [13](#)